SCIENCE CHINA
Information Sciences

• RESEARCH PAPER •

February 2026, Vol. 69, Iss. 2, 122304:1–122304:17
https://doi.org/10.1007/s11432-025-4640-y

Cooperative sensing and communication beamforming design for low-altitude economy

Fangzhi LI[1], Zhichu REN[1], Cunhua PAN[1*], Hong REN[1], Jing JIN[2], Qixing WANG[2] & Jiangzhou WANG[1*]

[1]*National Mobile Communications Research Laboratory, Southeast University, Nanjing 210096, China*
[2]*China Mobile Research Institute, Beijing 100045, China*

Received 24 May 2025/Revised 5 September 2025/Accepted 17 October 2025/Published online 6 January 2026

Abstract This paper proposes a cooperative integrated sensing and communication (ISAC) framework to support the low-altitude economy with high-accuracy sensing and high-rate communication. In the framework, ground base stations (BSs) use coordinated beamforming to cooperatively serve heterogeneous unmanned aerial vehicles (UAVs) performing either ISAC or sensing-only tasks. To maximize the weighted sum rate subject to sensing signal-to-interference-plus-noise ratio (SINR) constraints, we jointly optimize the BS transmit beamforming, UAV receive filtering, and UAV trajectories. An efficient alternating optimization algorithm, incorporating semidefinite relaxation (SDR) and successive convex approximation (SCA), is developed to solve the challenging non-convex problem. Simulation results demonstrate that the proposed joint cooperative design achieves superior communication throughput while ensuring sensing robustness, and underscore the necessity of adapting UAV trajectories to varying sensing requirements, BS transmit power and altitudes.

Keywords integrated sensing and communication (ISAC), low-altitude economy, unmanned aerial vehicle (UAV), beamforming, trajectory optimization

Citation Li F Z, Ren Z C, Pan C H, et al. Cooperative sensing and communication beamforming design for low-altitude economy. Sci China Inf Sci, 2026, 69(2): 122304, https://doi.org/10.1007/s11432-025-4640-y

1 Introduction

The evolution of sixth-generation (6G) wireless networks is driving a paradigm shift toward architectures that integrate communication and sensing functionalities. Integrated sensing and communication (ISAC), as a key enabler, utilizes shared spectrum and hardware to enable concurrent data transmission and environmental perception. This unified approach improves spectral efficiency, reduces system complexity, and enhances adaptability to dynamic environments [1–3]. It supports the convergence of functions and promotes compact, cost-effective system designs. ISAC has demonstrated strong potential in latency-sensitive applications such as intelligent transportation, emergency communication, and low-altitude surveillance [4]. The underlying physical layer is also evolving, with advanced waveforms based on orthogonal frequency division multiplexing (OFDM) being designed to strike an effective balance between communication capacity and sensing precision [5].

To enhance ISAC performance, cooperative architectures have attracted growing interest. Compared with single-node systems, cooperation among base stations (BSs) enables joint signal transmission and beamforming, which improves spatial resolution, suppresses interference, and enhances sensing accuracy [1,6]. Such cooperative frameworks, where different nodes might handle transmission and reception to mitigate challenges like self-interference, are a key area of study, with research exploring bistatic radar cross-section (RCS) analysis and synchronization to validate their feasibility [7]. Furthermore, advanced architectures like network-assisted full-duplex in cell-free networks are being investigated to support multi-static ISAC with coexisting uplink and downlink communications [8]. Such cooperation also facilitates resource pooling and information sharing, supporting robust ISAC in heterogeneous environments. In challenging scenarios with low signal-to-interference-plus-noise ratio (SINR), such as urban canyons, cooperation significantly improves detection of weak or distant targets [3,4]. Recent studies have further investigated integrated trajectory and resource scheduling for cooperative ISAC, laying the groundwork for algorithmic and system-level optimization [9].

* Corresponding author (email: cpan@seu.edu.cn, j.wang@seu.edu.cn)

Unmanned aerial vehicles (UAVs) have emerged as key components in cooperative ISAC systems due to their high mobility, flexible deployment, and favorable line-of-sight (LoS) conditions [2, 10, 11]. UAVs serve as aerial relays while performing sensing tasks such as detection, mapping, and tracking [11–13]. By dynamically adjusting trajectories, UAVs enhance air-ground link quality and extend sensing coverage to meet time-varying mission and channel requirements [14–16].

Motivated by these advantages, systems involving multiple BSs and heterogeneous UAVs are gaining momentum. In such systems, BSs jointly manage beamforming and signal scheduling to support UAV communications while improving sensing of passive targets [1, 17, 18]. UAV heterogeneity enables flexible task allocation. However, tight coupling between trajectories, beamforming, and sensing performance leads to complex, high-dimensional, and non-convex optimization problems, especially under real-time constraints [16, 19].

To tackle these challenges, joint optimization strategies have been proposed, combining trajectory planning with beamforming design. Some approaches adjust UAV positions to enhance channel conditions and beam alignment [10, 11, 18], while others incorporate advanced techniques such as 3D beamforming, time-domain tracking, and target motion prediction to improve reliability and sensing accuracy [20–22]. This includes operational strategies like resolution-aware beam scanning to effectively detect targets with required precision [23], as well as the development of fundamental performance metrics, such as task mutual information, to formally evaluate the capability for discrete sensing tasks [24]. Beam-assisted sensing has also been applied to enhance UAV localization and DoA estimation in dynamic and multipath-rich environments [25].

Energy-aware designs have integrated UAV power consumption models into trajectory planning, enabling energy-efficient beam and trajectory control frameworks [26]. These designs support performance-endurance trade-offs, especially for long-duration tasks. Deep reinforcement learning (DRL) has been applied for adaptive control under dynamic conditions such as mobility, jamming, or weather, though issues with scalability and interpretability remain [27]. This is part of a broader trend toward intelligent ISAC, where AI-driven, data-centric methods are increasingly utilized to tackle the high complexity of ISAC optimization problems that are often intractable for traditional model-based approaches [28]. For UAV-based ISAC systems specifically, machine learning provides a promising data-driven approach for designing end-to-end predictive beamforming schemes, directly mapping historical channel data to optimized beamforming matrices [29]. Reconfigurable intelligent surfaces (RIS) have also been explored, enabling controllable reflection paths that assist UAVs with beam steering and propagation enhancement [3, 30–38]. RIS expands spatial degrees of freedom and mitigates blockage effects in low-altitude scenarios. Integrating RIS into UAV-assisted ISAC allows fine-grained control and robust sensing, offering both theoretical and practical benefits for joint trajectory and beamforming design [33, 35]. An overview of different IRS architectures, including fully-passive, semi-passive, and active IRSs, highlights their distinct fundamental limits and roles in enabling non-line-of-sight sensing and communication [39].

Motivated by the aforementioned challenges and opportunities, this paper proposes a cooperative UAV-assisted ISAC system tailored for low-altitude economy (LAE) scenarios. The system includes two types of UAVs: those supporting both communication and sensing, and those dedicated to sensing. Ground BSs cooperatively transmit integrated signals via coordinated beamforming to provide communication services and perform target detection. A unified signal model is developed to capture key processes such as signal transmission, echo reception, self-interference, and receive filtering, enabling accurate characterization of heterogeneous UAVs and cooperative multi-BS operations. The main contributions are as follows.

- We establish a cooperative UAV-assisted ISAC system model tailored for low-altitude scenarios, where multiple BSs jointly serve heterogeneous UAVs. A unified signal model is developed to capture the processes of communication transmission, echo reception, and interference, and we derive closed-form expressions for both achievable communication rate and sensing SINR.
- A joint optimization problem is formulated to maximize the overall communication throughput while satisfying sensing quality requirements. The optimization variables include BS transmit beamformers, UAV receive filters, and UAV trajectories, subject to realistic constraints such as power limits, mobility dynamics, and collision avoidance.
- To efficiently solve the resulting non-convex problem, we design an alternating optimization algorithm that decomposes the problem into three submodules. Each subproblem is tackled using appropriate techniques such as semidefinite relaxation (SDR), successive convex approximation (SCA), Rayleigh quotient analysis, and trust-region methods to ensure convergence.
- Extensive simulations are conducted to evaluate the performance of the proposed method against baseline schemes. Results demonstrate significant gains in both communication and sensing metrics, and further sensitivity analysis offers insights into the impact of system parameters such as UAV altitude and BS density.

The rest of this paper is organized as follows. Section 2 describes the system model, including UAV architecture,

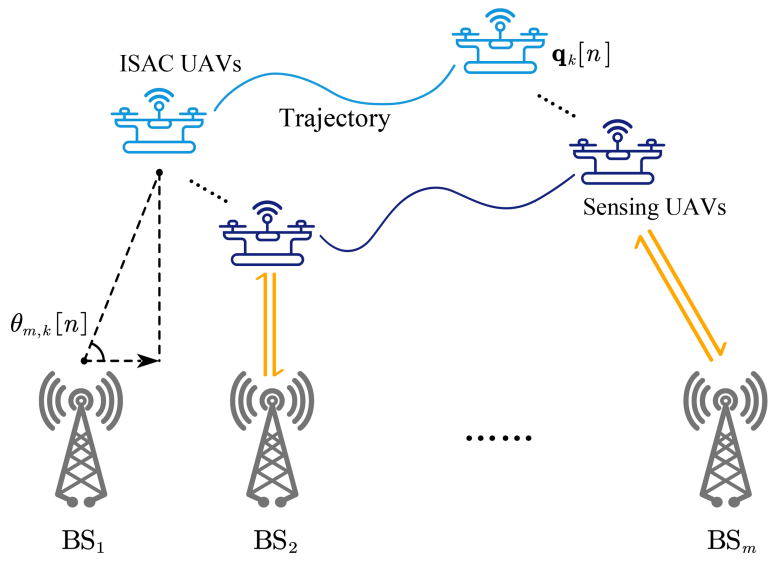

Figure 1 (Color online) System model.

signal modeling, and constraints. Section 3 presents the proposed solution, detailing the alternating optimization strategy and subproblem formulations. Section 4 reports simulation results and comparisons with benchmarks. Section 5 concludes the paper.

Notations: Lowercase and uppercase boldface letters represent vectors and matrices, respectively. $\mathbb{E}(\cdot)$ denotes statistical expectation. For a scalar a and a vector $\mathbf{a}$, $|a|$ and $\|\mathbf{a}\|$ represent the absolute value and Euclidean norm, respectively. Superscripts $(\cdot)^{\mathrm{T}}$ and $(\cdot)^{\mathrm{H}}$ denote transpose and Hermitian transpose. $\mathbb{C}^{x\times y}$ denotes the space of $x \times y$ complex matrices. $j = \sqrt{-1}$ denotes the imaginary unit.

2 System model

We consider a cooperative ISAC system, as illustrated in Figure 1, which comprises multiple ground BSs and two types of UAVs, each serving different operational roles. The first type, referred to as communication-and-sensing UAVs, is defined as the set $\mathcal{K}_{\mathrm{cs}} = \{1, \ldots, K_{\mathrm{cs}}\}$. These UAVs are equipped with a single antenna and can perform both wireless data exchange and environmental sensing simultaneously, making them highly versatile in mission-critical scenarios. The second type, defined as $\mathcal{K}_{\mathrm{s}} = \{1, \ldots, K_{\mathrm{s}}\}$, includes sensing-only UAVs, which act as passive point targets and focus exclusively on collecting environmental information without any communication hardware. The set of all UAVs is defined as $\mathcal{K} = \mathcal{K}_{\mathrm{cs}} \cup \mathcal{K}_{\mathrm{s}}$, with a combined cardinality of $K = K_{\mathrm{cs}} + K_{\mathrm{s}}$.

The ground infrastructure consists of M BSs, represented by the set $\mathcal{M} = \{1, 2, \ldots, M\}$. Each BS is equipped with a uniform linear antenna array (ULA) with L elements, enabling directional beamforming to support both communication and sensing. These BSs work cooperatively to serve the UAVs by transmitting integrated signals and processing returned echoes, thereby forming a tightly coupled aerial-ground ISAC network.

For time management, the system operates over a total period T, which is divided into N discrete and evenly spaced time slots. Each time slot has a duration defined as $\Delta t = \frac{T}{N}$. The collection of all these time slots is defined as the set $\mathcal{N} = \{1, 2, \ldots, N\}$, where N indicates the total number of time slots within the operational period. This discretized timeline facilitates efficient modeling of dynamic interactions between the UAVs and the ground system.

In a three-dimensional Cartesian coordinate system, the horizontal position of each BS $m \in \mathcal{M}$ is represented by a two-dimensional vector $\mathbf{v}_m = (x_m, y_m)$. Similarly, the position of the k-th UAV at the n-th time slot is characterized by its horizontal coordinates $\mathbf{q}_k[n] = (x_k[n], y_k[n])$ and its altitude H_k. The altitude H_k of UAV k is constrained within a specific range to ensure operational safety and compliance with system requirements:

$$H_{\min} \leqslant H_k \leqslant H_{\max}, \tag{1}$$

where $H_{\min}$ and $H_{\max}$ represent the minimum and maximum permissible altitudes, respectively.

At a specific time slot n, the angle of departure (AoD) from BS m to UAV k can be computed geometrically

based on the relative positions of the BS and UAV. The AoD $\theta_{m,k}[n]$ is given by

$$\theta_{m,k}[n] = \arccos\left(\frac{H_k}{\sqrt{\|\mathbf{q}_k[n] - \mathbf{v}_m\|^2 + H_k^2}}\right). \tag{2}$$

To facilitate signal processing, the steering vector corresponding to the calculated AoD $\theta_{m,k}[n]$ is defined as

$$\mathbf{a}_{m,k}[n] = [1, e^{2\pi\frac{d}{\lambda}\cos\theta_{m,k}[n]}, \ldots, e^{2\pi\frac{d}{\lambda}(L-1)\cos\theta_{m,k}[n]}]^{\mathrm{T}}, \tag{3}$$

where d denotes the antenna spacing, and λ is the wavelength of the transmitted signal.

Since the system operates in a low-altitude environment, non-line-of-sight (NLoS) paths are negligible. While this LoS assumption simplifies the analysis, it is important to note that comprehensive standardized models based on geometry-based stochastic methods (GBSM) are being developed to capture complex multipath effects by concatenating transmission and reflection channel segments in various ISAC scenarios [40]. For the scope of this work, only the LoS component is considered in the channel model, which captures the geometric relationship between the UAV and the n-th BS, as well as the effects of path loss and antenna steering.

The channel vector between BS m and UAV k at time slot n is given by

$$\mathbf{h}_{m,k}[n] = \sqrt{\beta_{m,k}[n]} \cdot \mathbf{a}_{m,k}[n], \tag{4}$$

where $\beta_{m,k}[n]$ represents the path loss associated with the signal propagation distance between BS m and UAV k. The path loss $\beta_{m,k}[n]$ is calculated as

$$\beta_{m,k}[n] = \kappa(\|\mathbf{q}_k[n] - \mathbf{v}_m\|^2 + H_k^2)^{-1}, \tag{5}$$

where κ is the reference path loss at a distance of 1 m.

By combining these expressions, the channel vector from BS m to UAV k can be expressed in its final form as

$$\mathbf{h}_{m,k}[n] = \kappa^{\frac{1}{2}}(\|\mathbf{q}_k[n] - \mathbf{v}_m\|^2 + H_k^2)^{-\frac{1}{2}} \cdot \mathbf{a}_{m,k}[n]. \tag{6}$$

2.1 Communication model

In the proposed system, the ground BSs work cooperatively to establish robust communication links with UAVs while simultaneously supporting sensing tasks. This cooperative operation enables the efficient use of spectrum and resources, ensuring that both communication and sensing requirements are fulfilled in real time. Each BS is responsible for transmitting signals that serve both communication and sensing purposes, allowing the system to adapt dynamically to the demands of the UAV network.

The total transmitted signal of BS m at time slot n is given by

$$\mathbf{x}_m[n] = \sum_{i\in\mathcal{K}_{cs}} \mathbf{w}_{m,i}^c[n] s_{m,i}^c[n] + \sum_{i\in\mathcal{K}} \mathbf{w}_{m,i}^r[n] s_{m,i}^r[n], \tag{7}$$

where $s_{m,i}^c[n]$ and $s_{m,i}^r[n]$ denote the communication and sensing symbols transmitted from BS m to UAV i, respectively, and $\mathbf{w}_{m,i}^c[n], \mathbf{w}_{m,i}^r[n] \in \mathbb{C}^{L\times 1}$ are the corresponding beamforming vectors.

The communication signal received by UAV k at time slot n is a superposition of signals transmitted from all BSs, including the desired communication signal, interference from other users' communication signals, and interference from sensing signals. This received signal can be expressed as

$$\mathbf{y}_k[n] = \underbrace{\sum_{m\in\mathcal{M}} \mathbf{h}_{m,k}^{\mathrm{H}}[n]\mathbf{w}_{m,k}^c[n]s_{m,k}^c[n]}_{\text{desired signal}} + \underbrace{\sum_{m\in\mathcal{M}}\sum_{i\in\mathcal{K}_{cs}\setminus k} \mathbf{h}_{m,k}^{\mathrm{H}}[n]\mathbf{w}_{m,i}^c[n]s_{m,i}^c[n]}_{\text{multi-UAV interference}} + \underbrace{\sum_{m\in\mathcal{M}}\sum_{i\in\mathcal{K}} \mathbf{h}_{m,k}^{\mathrm{H}}[n]\mathbf{w}_{m,i}^r[n]s_{m,i}^r[n]}_{\text{sensing interference}} + \mathbf{n}_k[n], \tag{8}$$

where $\mathbf{n}_k[n] \sim \mathcal{CN}(0, \sigma^2\mathbf{I})$ denotes additive white Gaussian noise (AWGN) at the receiver.

Based on the received signal structure, the SINR for UAV k at time slot n is defined as

$$\gamma_k^c[n] = \frac{\sum_{m\in\mathcal{M}} |\mathbf{h}_{m,k}^{\mathrm{H}}[n]\mathbf{w}_{m,k}^c[n]|^2}{\sum_{m\in\mathcal{M}}\sum_{i\in\mathcal{K}_{cs}\setminus k} |\mathbf{h}_{m,k}^{\mathrm{H}}[n]\mathbf{w}_{m,i}^c[n]|^2 + \sum_{m\in\mathcal{M}}\sum_{i\in\mathcal{K}} |\mathbf{h}_{m,k}^{\mathrm{H}}[n]\mathbf{w}_{m,i}^r[n]|^2 + \sigma^2}. \tag{9}$$

The achievable communication rate $R_k[n]$ for UAV k during time slot n is derived based on the SINR $\gamma_k^c[n]$, which can be expressed as

$$R_k[n] = \log_2(1 + \gamma_k^c[n]). \tag{10}$$

To evaluate the overall communication performance of the system, the sum communication rate $R[n]$ for all UAVs at time slot n is defined as

$$R[n] = \sum_{k\in\mathcal{K}} \omega_k R_k[n] = \sum_{k\in\mathcal{K}} \omega_k \log_2(1 + \gamma_k^c[n]), \tag{11}$$

where ω_k is a weight factor that reflects the priority or importance of UAV k in the system. By appropriately choosing ω_k, the system can prioritize certain UAVs based on their mission-critical requirements or service demands.

This communication model provides a comprehensive framework for analyzing the performance of cooperative communication and sensing systems involving multiple BSs and UAVs. It accounts for interference, noise, and the impact of beamforming on the quality of the communication links.

2.2 Sensing model

In the proposed system, we consider a scenario where each UAV is sensed by the BSs using echo signal processing techniques. The sensing task involves detecting and tracking the UAVs, leveraging the reflected signals received at the BSs. The system adopts a cooperative sensing framework, wherein multiple BSs operate under a monostatic architecture and perform sensing individually via their own transmit and receive signals.

The received signal at BS j at time slot n can be expressed as

$$\mathbf{y}_{r,j}[n] = \underbrace{\sum_{l\in\mathcal{K}} \xi_{j,l}\mathbf{A}_{j,l}[n]\mathbf{x}_j[n]}_{\text{echo signals from UAVs}} + \underbrace{\sqrt{\zeta_j}\mathbf{H}_{\mathrm{SI},j}^{\mathrm{H}}\mathbf{x}_j[n]}_{\text{self-interference}} + \underbrace{\sum_{i\neq j, i\in\mathcal{M}} \sqrt{\alpha_{i,j}}\mathbf{G}_{i,j}^{\mathrm{H}}\mathbf{x}_i[n]}_{\text{inter-BS interference}} + \mathbf{n}_{r,j}, \tag{12}$$

where $\xi_{j,l} \sim \mathcal{CN}(0, \sigma_t^2)$ denotes the RCS of UAV l, and $\mathbf{A}_{j,l}[n]$ is the target response matrix defined as

$$\mathbf{A}_{j,l}[n] = \sqrt{\rho_{j,l}[n]} \cdot \mathbf{a}_{j,l}[n]\mathbf{a}_{j,l}^{\mathrm{H}}[n], \tag{13}$$

where $\rho_{j,l}[n]$ represents the path loss for the link between BS j and UAV l. The coefficient ζ_j characterizes the residual self-interference level, and the suppression coefficient $\alpha_{i,j}$ denotes the interference signal from BS i to BS j. The matrix $\mathbf{H}_{\mathrm{SI},j} \in \mathbb{C}^{L\times L}$ is the self-interference channel matrix of BS j, the matrix $\mathbf{G}_{i,j}$ represents the direct channel from BS i to BS j, and $\mathbf{n}_{r,j} \sim \mathcal{CN}(0, \sigma_r^2\mathbf{I}_L)$ is the additive Gaussian noise.

To isolate the reflected signals of interest, each BS applies a receive filter $\mathbf{u}_{j,k}[n] \in \mathbb{C}^{L\times 1}$. The filtered echo signal corresponding to UAV k, received by BS j, is given by

$$\mathbf{u}_{j,k}^{\mathrm{H}}[n]\mathbf{y}_{r,j}[n] = \mathbf{u}_{j,k}^{\mathrm{H}}[n]\sum_{l\in\mathcal{K}}\xi_{j,l}\mathbf{A}_{j,l}[n]\mathbf{x}_j[n] + \mathbf{u}_{j,k}^{\mathrm{H}}[n]\sqrt{\zeta_j}\mathbf{H}_{\mathrm{SI},j}^{\mathrm{H}}\mathbf{x}_j[n] + \mathbf{u}_{j,k}^{\mathrm{H}}[n]\sum_{i\neq j, i\in\mathcal{M}}\sqrt{\alpha_{i,j}}\mathbf{G}_{i,j}^{\mathrm{H}}\mathbf{x}_i[n] + \mathbf{u}_{j,k}^{\mathrm{H}}[n]\mathbf{n}_{r,j}. \tag{14}$$

The total filtered echo signal received by all BSs for UAV k is represented as $\sum_{j\in\mathcal{M}}\mathbf{u}_{j,k}^{\mathrm{H}}[n]\mathbf{y}_{r,j}[n]$. Based on the filtered and aggregated echo signals, the sensing SINR serves as a key metric to evaluate the quality of the sensing performance for UAV k at time slot n. The corresponding SINR, denoted by $\gamma_k^r[n]$, quantifies the ratio of the power of the desired echo signals to that of the combined interference and noise. Its explicit expression is provided in (15).

$$\gamma_k^r[n] = \frac{\sigma_t^2\mathbb{E}\Big[\sum\limits_{j\in\mathcal{M}}\Big|\mathbf{u}_{j,k}^{\mathrm{H}}[n]\xi_{j,k}\mathbf{A}_{j,k}[n]\mathbf{x}_j[n]\Big|^2\Big]}{\zeta_j\mathbb{E}\Big[\sum\limits_{j\in\mathcal{M}}\Big|\mathbf{u}_{j,k}^{\mathrm{H}}[n]\mathbf{H}_{\mathrm{SI},j}^{\mathrm{H}}\mathbf{x}_j[n]\Big|^2\Big] + \alpha_{i,j}\mathbb{E}\Big[\sum\limits_{j\in\mathcal{M}}\sum\limits_{i\neq j}\Big|\mathbf{u}_{j,k}^{\mathrm{H}}[n]\mathbf{G}_{i,j}^{\mathrm{H}}\mathbf{x}_i[n]\Big|^2\Big] + \sigma_r^2\sum\limits_{j\in\mathcal{M}}\Big\|\mathbf{u}_{j,k}[n]\Big\|^2 + \sigma_t^2\mathbb{E}\Big[\sum\limits_{j\in\mathcal{M}}\sum\limits_{l\neq k}\Big|\mathbf{u}_{j,k}^{\mathrm{H}}[n]\xi_{j,l}\mathbf{A}_{j,l}[n]\mathbf{x}_j[n]\Big|^2\Big]}. \tag{15}$$

2.3 Problem formulation

In the proposed ISAC system, we jointly optimize the coordinated transmit beamforming vectors $\{\mathbf{w}_{m,k}^c[n]\}$ and $\{\mathbf{w}_{m,k}^r[n]\}$, the receive filters $\{\mathbf{u}_{j,k}[n]\}$, and the UAV trajectories $\{\mathbf{q}_k[n]\}$. The objective is to maximize the weighted sum rate while ensuring that the sensing SINR for all UAVs at each time slot exceeds a predefined threshold Γ. This formulation captures the trade-off between communication and sensing, aligning with the ISAC paradigm.

Since the UAVs are assigned predefined initial and final positions within the total operational period T, their trajectories must comply with the following position constraints:

$$\mathbf{q}_k[1] = \mathbf{q}_k^{\mathrm{I}}, \tag{16}$$

$$\mathbf{q}_k[n] = \mathbf{q}_k^{\mathrm{F}}, \tag{17}$$

where $\mathbf{q}_k^{\mathrm{I}}$ and $\mathbf{q}_k^{\mathrm{F}}$ denote the fixed initial and final horizontal positions of UAV k, respectively. These constraints ensure that each UAV begins its mission from a designated starting location and eventually reaches its assigned destination, which may be determined by mission planning, airspace coordination, or task-specific requirements.

In addition to the initial and terminal position requirements, UAV trajectories must satisfy physical motion constraints and safety requirements throughout the flight. In particular, each UAV must comply with a maximum speed limit and maintain a safe distance from other UAVs to avoid potential collisions. The constraints are specified as follows:

$$\|\mathbf{q}_k[n+1] - \mathbf{q}_k[n]\|^2 \leqslant V_{\max}\Delta t, \quad \forall k \in \mathcal{K},\, n \in \mathcal{N}, \tag{18}$$

$$\|\mathbf{q}_j[n] - \mathbf{q}_i[n]\|^2 + (H_j - H_i)^2 \geqslant D_{\min}^2, \forall j, i \in \mathcal{K}, j \neq i, n \in \mathcal{N}, \tag{19}$$

where $V_{\max}$ represents the maximum allowable speed of a UAV, and Δt is the fixed time duration of each slot. The parameter $D_{\min}$ denotes the minimum safe distance that must be maintained between any two UAVs at all times, taking into account their three-dimensional positions through the inclusion of altitude differences. These constraints are essential to ensure that UAV trajectories are not only dynamically feasible under motion limits, but also satisfy airspace safety requirements to prevent mid-air collisions.

Furthermore, to maintain energy efficiency and ensure practical deployment, the total transmit power of each BS must be kept within a predefined power budget $P_{\max}$. Accordingly, the transmit power constraint for BS m at time slot n is given by

$$\sum_{k \in \mathcal{K}_{cs}} \|\mathbf{w}_{m,k}^c[n]\|^2 + \sum_{k \in \mathcal{K}} \|\mathbf{w}_{m,k}^r[n]\|^2 \leqslant P_{\max}, \quad \forall m, n. \tag{20}$$

This constraint ensures that the sum power allocated to both communication and sensing signals by BS m does not exceed its maximum transmission capacity. It serves to regulate energy consumption, promote sustainable operation, and prevent signal distortion due to hardware limitations.

Given the constraints above, the joint coordinated transmit beamforming and UAV trajectory optimization problem can be formulated as follows:

$$(\mathrm{P1}): \max_{\{\mathbf{w}_{m,k}^c[n], \mathbf{w}_{m,k}^r[n], \mathbf{u}_{j,k}[n], \mathbf{q}_k[n]\}} \sum_{n \in \mathcal{N}} R[n] \tag{21a}$$

$$\text{s.t.} \quad \gamma_k^r[n] \geqslant \Gamma, \quad \forall k, n, \tag{21b}$$

$$\sum_{k \in \mathcal{K}_{cs}} \|\mathbf{w}_{m,k}^c[n]\|^2 + \sum_{k \in \mathcal{K}} \|\mathbf{w}_{m,k}^r[n]\|^2 \leqslant P_{\max}, \quad \forall m, n, \tag{21c}$$

$$\mathbf{q}_k[1] = \mathbf{q}_k^{\mathrm{I}}, \tag{21d}$$

$$\mathbf{q}_k[N] = \mathbf{q}_k^{\mathrm{F}}, \tag{21e}$$

$$\|\mathbf{q}_k[n+1] - \mathbf{q}_k[n]\|^2 \leqslant V_{\max}\Delta t, \quad \forall k \in \mathcal{K}, n \in \mathcal{N}, \tag{21f}$$

$$\|\mathbf{q}_j[n] - \mathbf{q}_i[n]\|^2 + (H_j - H_i)^2 \geqslant D_{\min}^2, \quad \forall j, i \in \mathcal{K}, j \neq i, n \in \mathcal{N}. \tag{21g}$$

In this formulation, the objective in (21a) maximizes the total communication rate $R[n]$ over all UAVs and time slots. Constraint (21b) ensures that the sensing SINR $\gamma_k^r[n]$ exceeds a threshold Γ for reliable sensing. The power constraint (21c) limits each BS's transmit power to manage energy consumption. Constraints (21d) and (21e) specify the UAVs' initial and final positions, while constraint (21f) enforces a speed limit on UAV movement between time slots. Eventually, constraint (21g) imposes a minimum separation distance $D_{\min}$ to prevent collisions.

Problem (P1) is a non-convex optimization involving coupled variables—beamforming vectors, receive filters, and UAV trajectories—with non-linear, bilinear, and quadratic terms in both the objective and constraints. Rank-one constraints and the coupling between beamforming and mobility further increase complexity and render the problem NP-hard. Due to the intractability of closed-form solutions, we propose an alternating optimization framework that decomposes the problem into subproblems, each solved iteratively using convex techniques such as SDR and SCA.

3 Proposed solution

In this section, we address the joint optimization problem (P1). Due to the complexity of jointly optimizing transmit beamforming $\{\mathbf{w}^c_{m,k}[n]\}$ and $\{\mathbf{w}^r_{m,k}[n]\}$, receive filters $\{\mathbf{u}_{j,k}[n]\}$, and UAV trajectories $\{\mathbf{q}_k[n]\}$, we adopt an alternating optimization framework combined with the SCA technique. This approach updates each variable while fixing the others, and converges to a locally optimal solution.

3.1 Problem reformulation

From the expression in (7), the filtered echo signal for UAV k received by BS j at time slot n can be decomposed as

$$\mathbf{u}^{\mathrm{H}}_{j,k}[n]\mathbf{A}_{j,k}[n]\mathbf{x}_j[n] = \sum_{t\in\mathcal{K}_{cs}} \mathbf{u}^{\mathrm{H}}_{j,k}[n]\mathbf{A}_{j,k}[n]\mathbf{w}^c_{j,t}[n]s^c_{j,t}[n] + \sum_{t\in\mathcal{K}} \mathbf{u}^{\mathrm{H}}_{j,k}[n]\mathbf{A}_{j,k}[n]\mathbf{w}^r_{j,t}[n]s^r_{j,t}[n]. \tag{22}$$

Using the orthogonality and power normalization properties of the transmitted signals, i.e., $\mathbb{E}[|s|^2] = 1$, we compute the covariance matrix of the transmitted signal $\mathbf{x}_j[n]$ as

$$\mathbf{X}_j[n] = \mathbb{E}[\mathbf{x}_j[n]\mathbf{x}^{\mathrm{H}}_j[n]] = \sum_{t\in\mathcal{K}_{cs}} \mathbf{w}^c_{j,t}[n](\mathbf{w}^c_{j,t}[n])^{\mathrm{H}} + \sum_{t\in\mathcal{K}} \mathbf{w}^r_{j,t}[n](\mathbf{w}^r_{j,t}[n])^{\mathrm{H}}. \tag{23}$$

Thus, the numerator of the sensing SINR $\gamma^r_k[n]$ is given by $\sigma_t^2 \sum_{j\in\mathcal{M}} \mathbf{u}^{\mathrm{H}}_{j,k}[n]\mathbf{A}_{j,k}[n]\mathbf{X}_j[n]\mathbf{A}^{\mathrm{H}}_{j,k}[n]\mathbf{u}_{j,k}[n]$.

Through applying linear filtering, matrix trace properties, and substituting the signal covariance matrix $\mathbf{X}_j[n]$, the interference and noise terms in the denominator of $\gamma^r_k[n]$ can be reformulated in a compact quadratic form. As a result, the sensing SINR expression is equivalently rewritten as

$$\gamma^r_k[n] = \frac{\sigma_t^2 \sum\limits_{j\in\mathcal{M}} \mathbf{u}^{\mathrm{H}}_{j,k}[n]\mathbf{A}_{j,k}[n]\mathbf{X}_j[n]\mathbf{A}^{\mathrm{H}}_{j,k}[n]\mathbf{u}_{j,k}[n]}{\sum\limits_{j\in\mathcal{M}} \mathbf{u}^{\mathrm{H}}_{j,k}[n]\left(\zeta_j\mathbf{H}_{\mathrm{SI},j}\mathbf{X}_j[n]\mathbf{H}^{\mathrm{H}}_{\mathrm{SI},j} + \alpha_{i,j}\sum\limits_{i\neq j, i\in\mathcal{M}} \mathbf{G}_{i,j}\mathbf{X}_i[n]\mathbf{G}^{\mathrm{H}}_{i,j} + \sigma_r^2\mathbf{I}_L + \sigma_t^2\sum\limits_{l\neq k, l\in\mathcal{K}} \mathbf{A}_{j,l}[n]\mathbf{X}_j[n]\mathbf{A}^{\mathrm{H}}_{j,l}[n]\right)\mathbf{u}_{j,k}[n]}. \tag{24}$$

By defining $\mathbf{H}_{m,k}[n] = \mathbf{h}_{m,k}[n]\mathbf{h}^{\mathrm{H}}_{m,k}[n]$, and introducing the beamforming covariance matrices as $\mathbf{W}^c_{m,k}[n] = \mathbf{w}^c_{m,k}[n](\mathbf{w}^c_{j,t}[n])^{\mathrm{H}}$ and $\mathbf{W}^r_{m,k}[n] = \mathbf{w}^r_{m,k}[n](\mathbf{w}^r_{j,t}[n])^{\mathrm{H}}$, where $\mathbf{W}^c_{m,k}[n] \succeq 0$, $\mathbf{W}^r_{m,k}[n] \succeq 0$, and $\mathrm{rank}(\mathbf{W}^c_{m,k}[n]) = 1$, the transmit signal covariance matrix $\mathbf{X}_j[n]$ can be equivalently expressed as

$$\mathbf{X}_j[n] = \sum_{t\in\mathcal{K}_{cs}} \mathbf{W}^c_{j,t}[n] + \sum_{t\in\mathcal{K}} \mathbf{W}^r_{j,t}[n], \tag{25}$$

where $\mathbf{X}_j[n] \succeq 0$ and each term in the summation corresponds to the contribution from either communication or sensing beamforming signals.

With these reformulations, problem (P1) can be equivalently transformed into problem (P2) as follows:

$$(\mathrm{P2}): \max_{\{\mathbf{W}^c_{m,k}[n], \mathbf{W}^r_{m,k}[n], \mathbf{u}_{j,k}[n], \mathbf{q}_k[n]\}} \sum_{n\in\mathcal{N}}\sum_{k\in\mathcal{K}} \omega_k \bar{R}_k[n] \tag{26a}$$

$$\text{s.t.} \quad \sum_{k\in\mathcal{K}_{cs}} \mathrm{tr}(\mathbf{W}^c_{m,k}[n]) + \sum_{k\in\mathcal{K}} \mathrm{tr}(\mathbf{W}^r_{m,k}[n]) \leqslant P_{\max},\ \forall m, n, \tag{26b}$$

$$\mathrm{rank}(\mathbf{W}^c_{m,k}[n]) = 1,\ \forall m, k, n, \tag{26c}$$

$$(21\mathrm{b}),\ (21\mathrm{d}),\ (21\mathrm{e}),\ (21\mathrm{f}),\ (21\mathrm{g}).$$

To solve problem (P2), we adopt the alternating optimization (AO)-based algorithm, iteratively optimizing one set of variables while fixing the others.

3.2 Transmit beamforming optimization

In this section, we propose an efficient algorithm to address problem (P2), focusing on optimizing the communication and sensing beamforming matrices $\mathbf{W}^c_{m,k}[n]$ and $\mathbf{W}^r_{m,k}[n]$. The optimization is performed under fixed filter designs

$\mathbf{u}_{j,k}[n]$ and UAV trajectories $\mathbf{q}_k[n]$. By carefully analyzing the structure of the problem, it can be seen that optimizing the beamforming is equivalent to solving the problem (P3) as follows:

$$\begin{aligned}(\text{P3}): &\max_{\{\mathbf{W}^c_{m,k}[n],\mathbf{W}^r_{m,k}[n]\}} \sum_{n\in\mathcal{N}} R[n]\\ &\text{s.t. (21b), (26b), (26c).}\end{aligned}$$

Constraint (26b), which represents the power budget at each BS, is straightforwardly convex as it is linear in terms of the optimization variables $\mathbf{W}^c_{m,k}[n]$ and $\mathbf{W}^r_{m,k}[n]$. To verify whether constraint (21b) is convex, we reformulate it as the inequality in (27).

$$\begin{aligned}&\sigma_t^2 \sum_{j\in\mathcal{M}} \mathbf{u}^{\mathrm{H}}_{j,k}[n]\mathbf{A}_{j,k}[n]\mathbf{X}_j[n]\mathbf{A}^{\mathrm{H}}_{j,k}[n]\mathbf{u}_{j,k}[n]\\ \geqslant&\Gamma\cdot\Bigg\{\sum_{j\in\mathcal{M}} \mathbf{u}^{\mathrm{H}}_{j,k}[n]\Big(\zeta_j\mathbf{H}_{\mathrm{SI},j}\mathbf{X}_j[n]\mathbf{H}^{\mathrm{H}}_{\mathrm{SI},j}+\alpha_{i,j}\sum_{\substack{i\neq j,\\ i\in\mathcal{M}}}\mathbf{G}_{i,j}\mathbf{X}_i[n]\mathbf{G}^{\mathrm{H}}_{i,j}+\sigma_r^2\mathbf{I}_L+\sigma_t^2\sum_{\substack{l\neq k,\\ l\in\mathcal{K}}}\mathbf{A}_{j,l}[n]\mathbf{X}_j[n]\mathbf{A}^{\mathrm{H}}_{j,l}[n]\Big)\mathbf{u}_{j,k}[n]\Bigg\}.\end{aligned}\tag{27}$$

It can be observed that this constraint is linear with respect to $\mathbf{X}_j[n]$. Since $\mathbf{X}_j[n]$ is a jointly convex function of $\mathbf{W}^c_{m,k}[n]$ and $\mathbf{W}^r_{m,k}[n]$, it follows that constraint (21b) is also convex with respect to these variables.

Although constraints (21b) and (26b) are convex, the objective function $R[n]$ and the rank constraint (26c) introduce non-convexity into problem (P3). To address this challenge, the SCA method is applied, where the non-convex components of the objective function are approximated with convex surrogates in each iteration.

Let $\mathbf{W}^{c(f)}_{m,k}[n]$ and $\mathbf{W}^{r(f)}_{m,k}[n]$ denote the current local point at the f-th iteration, $f\geqslant 1$. During each iteration, the logarithmic terms in the objective function are linearized around the current solution. This linearization results in a convex approximation of the objective function, which can then be solved efficiently using standard convex optimization techniques. By iteratively updating the beamforming matrices and solving the resulting subproblems, the algorithm converges to a high-quality locally optimal solution. To illustrate this, the communication SINR $\gamma^c_k[n]$ can be re-expressed as

$$\gamma^c_k[n]=\frac{\sum\limits_{m\in\mathcal{M}}\mathrm{tr}(\mathbf{H}_{m,k}[n]\mathbf{W}^c_{m,k}[n])}{\sum\limits_{m\in\mathcal{M}}\sum\limits_{i\in\mathcal{K}_{cs}\backslash k}\mathrm{tr}(\mathbf{H}_{m,k}[n]\mathbf{W}^c_{m,i}[n])+\sum\limits_{m\in\mathcal{M}}\sum\limits_{i\in\mathcal{K}}\mathrm{tr}(\mathbf{H}_{m,k}[n]\mathbf{W}^r_{m,i}[n])+\sigma^2}.\tag{28}$$

The achievable rate $R_k[n]$ for UAV k at time slot n can then be expressed as

$$\begin{aligned}R_k[n]=&\log_2(1+\gamma^c_k[n])=\log_2\Bigg(\sum_{m\in\mathcal{M}}\sum_{i\in\mathcal{K}_{cs}}\mathrm{tr}(\mathbf{H}_{m,k}[n]\mathbf{W}^c_{m,i}[n])+\sum_{m\in\mathcal{M}}\sum_{i\in\mathcal{K}}\mathrm{tr}(\mathbf{H}_{m,k}[n]\mathbf{W}^r_{m,i}[n])+\sigma^2\Bigg)\\ &-\log_2\Bigg(\sum_{m\in\mathcal{M}}\sum_{i\in\mathcal{K}_{cs}\backslash k}\mathrm{tr}(\mathbf{H}_{m,k}[n]\mathbf{W}^c_{m,i}[n])+\sum_{m\in\mathcal{M}}\sum_{i\in\mathcal{K}}\mathrm{tr}(\mathbf{H}_{m,k}[n]\mathbf{W}^r_{m,i}[n])+\sigma^2\Bigg).\end{aligned}\tag{29}$$

To address the non-convexity arising from the difference of logarithmic functions in (29), we employ the first-order Taylor expansion to approximate the second logarithmic term at a feasible point $(\mathbf{W}^{c(f)}_{m,i}[n],\mathbf{W}^{r(f)}_{m,i}[n])$. This yields a concave lower bound for the achievable rate $R_k[n]$, expressed as

$$\begin{aligned}R_k[n]\geqslant&\log_2\Bigg(\sum_{m\in\mathcal{M}}\sum_{i\in\mathcal{K}_{cs}}\mathrm{tr}(\mathbf{H}_{m,k}[n]\mathbf{W}^c_{m,i}[n])+\sum_{m\in\mathcal{M}}\sum_{i\in\mathcal{K}}\mathrm{tr}(\mathbf{H}_{m,k}[n]\mathbf{W}^r_{m,i}[n])+\sigma^2\Bigg)-a^{(f)}_k[n]\\ &-\sum_{m\in\mathcal{M}i\in\mathcal{K}_{cs}\backslash k}\mathrm{tr}(\mathbf{B}^{(f)}_{m,k}[n](\mathbf{W}^c_{m,i}[n]-\mathbf{W}^{c(f)}_{m,i}[n]))-\sum_{m\in\mathcal{M}}\sum_{i\in\mathcal{K}_{cs}}\mathrm{tr}(\mathbf{B}^{(f)}_{m,k}[n](\mathbf{W}^r_{m,i}[n]-\mathbf{W}^{r(f)}_{m,i}[n]))\triangleq\bar{R}_k[n],\end{aligned}\tag{30}$$

where

$$a^{(f)}_k[n]=\log_2\Bigg(\sum_{m\in\mathcal{M}}\sum_{i\in\mathcal{K}_{cs}\backslash k}\mathrm{tr}(\mathbf{H}_{m,k}[n]\mathbf{W}^{c(f)}_{m,i}[n])+\sum_{m\in\mathcal{M}}\sum_{i\in\mathcal{K}}\mathrm{tr}(\mathbf{H}_{m,k}[n]\mathbf{W}^{r(f)}_{m,i}[n])+\sigma^2\Bigg),\tag{31}$$

$$\mathbf{B}_{m,k}^{(f)}[n]=\frac{\log_2 e\cdot\mathbf{H}_{m,k}[n]}{\sum\limits_{m\in\mathcal{M}}\sum\limits_{i\in\mathcal{K}_{cs}\backslash k}\mathrm{tr}(\mathbf{H}_{m,k}[n]\mathbf{W}_{m,i}^{c(f)}[n])+\sum\limits_{m\in\mathcal{M}}\sum\limits_{i\in\mathcal{K}}\mathrm{tr}(\mathbf{H}_{m,k}[n]\mathbf{W}_{m,i}^{r(f)}[n])+\sigma^2}. \tag{32}$$

Based on the concave lower bound $\bar{R}_k[n]$, the original weighted sum rate maximization problem can be approximated by the following convex surrogate problem:

$$\begin{aligned}(\mathrm{P4}):\ &\max_{\{\mathbf{W}_{m,k}^{c}[n],\mathbf{W}_{m,k}^{r}[n]\}}\sum_{n\in\mathcal{N}}\bar{R}[n]\\ &\text{s.t. (21b), (26b), (26c).}\end{aligned}$$

However, the rank-one constraint (26c) in (P4) remains non-convex. To address this, the SDR method is employed, which relaxes the rank-one constraint and transforms (P4) into a standard convex optimization problem, referred to as (P4.SDR). The relaxed problem can be solved via CVX tools, yielding solutions $\mathbf{W}_{m,k}^{c*}[n]$ and $\mathbf{W}_{m,k}^{r*}[n]$. If these solutions are not rank-one, equivalent rank-one approximations are constructed as follows:

$$\bar{\mathbf{w}}_{m,i}^{c}[n]=\frac{\mathbf{W}_{m,i}^{c*}[n]\mathbf{h}_{m,k}[n]}{\sqrt{\mathbf{h}_{m,k}^{\mathrm{H}}[n]\mathbf{W}_{m,i}^{c*}[n]\mathbf{h}_{m,k}[n]}}, \tag{33}$$

$$\bar{\mathbf{W}}_{m,i}^{c}[n]=\bar{\mathbf{w}}_{m,i}^{c}[n]\cdot(\bar{\mathbf{w}}_{m,i}^{c}[n])^{\mathrm{H}}, \tag{34}$$

$$\bar{\mathbf{W}}_{m,i}^{r}[n]=\sum_{i\in\mathcal{K}}\mathbf{W}_{m,i}^{c*}[n]+\bar{\mathbf{W}}_{m,i}^{r*}[n]-\sum_{i\in\mathcal{K}}\bar{\mathbf{W}}_{m,i}^{c}[n]. \tag{35}$$

These solutions are rank-one and feasible for (P4) [3], and they achieve the same objective value as the relaxed problem (P4.SDR), ensuring that the relaxation is tight. This iterative process guarantees convergence to a high-quality locally optimal solution.

3.3 Receive filter optimization

In this section, we focus on optimizing the receive filter $\mathbf{u}_{j,k}[n]$ under the given beamforming matrices $\mathbf{W}_{m,k}^{c}[n]$ and $\mathbf{W}_{m,k}^{r}[n]$, as well as the fixed UAV trajectory $\mathbf{q}_k[n]$.

To begin with, the sensing SINR $\gamma_k^r[n]$ can be reformulated as

$$\gamma_k^r[n]=\sum_{j\in\mathcal{M}}\frac{\mathbf{u}_{j,k}^{\mathrm{H}}[n]\mathbf{E}_{j,k}[n]\mathbf{u}_{j,k}[n]}{\mathbf{u}_{j,k}^{\mathrm{H}}[n]\mathbf{F}_{j,k}[n]\mathbf{u}_{j,k}[n]}, \tag{36}$$

where the matrices $\mathbf{E}_{j,k}[n]$ and $\mathbf{F}_{j,k}[n]$ are defined as follows:

$$\mathbf{E}_{j,k}[n]=\sigma_t^2\mathbf{A}_{j,k}[n]\mathbf{X}_j[n]\mathbf{A}_{j,k}^{\mathrm{H}}[n], \tag{37}$$

$$\mathbf{F}_{j,k}[n]=\zeta_j\mathbf{H}_{\mathrm{SI},j}\mathbf{X}_j[n]\mathbf{H}_{\mathrm{SI},j}^{\mathrm{H}}+\sum_{i\neq j,i\in\mathcal{M}}\alpha_{i,j}\mathbf{G}_{i,j}\mathbf{X}_i[n]\mathbf{G}_{i,j}^{\mathrm{H}}+\sigma_r^2\mathbf{I}_L+\sigma_t^2\sum_{l\neq k,l\in\mathcal{K}}\mathbf{A}_{j,l}[n]\mathbf{X}_j[n]\mathbf{A}_{j,l}^{\mathrm{H}}[n]. \tag{38}$$

$\mathbf{E}_{j,k}[n]$ represents the covariance of the desired echo signals for UAV k, and $\mathbf{F}_{j,k}[n]$ is the covariance matrix of the interference and noise. Both $\mathbf{E}_{j,k}[n]$ and $\mathbf{F}_{j,k}[n]$ are both semi-positive Hermitian matrices.

The optimization of the receive filter $\mathbf{u}_{j,k}[n]$ can be formulated as follows:

$$\begin{aligned}(\mathrm{P5}):\quad &\max_{\{\mathbf{u}_{j,k}[n]\}}\sum_{n\in\mathcal{N}}R[n]\\ &\text{s.t.}\quad\sum_{j\in\mathcal{M}}\frac{\mathbf{u}_{j,k}^{\mathrm{H}}[n]\mathbf{E}_{j,k}[n]\mathbf{u}_{j,k}[n]}{\mathbf{u}_{j,k}^{\mathrm{H}}[n]\mathbf{F}_{j,k}[n]\mathbf{u}_{j,k}[n]}\geqslant\Gamma.\end{aligned} \tag{39}$$

The expression of the sensing SINR $\gamma_k^r[n]$ is in the form of a generalized Rayleigh quotient, where both the numerator and denominator are quadratic forms in $\mathbf{u}_{j,k}[n]$. It is well known that the optimal solution to such a quotient is achieved when $\mathbf{u}_{j,k}[n]$ is the dominant (i.e., principal) eigenvector of the matrix $\mathbf{F}_{j,k}^{-1/2}[n]\mathbf{E}_{j,k}[n]\mathbf{F}_{j,k}^{-1/2}[n]$, and the corresponding optimal value of the sensing SINR equals the largest eigenvalue.

Therefore, to satisfy the sensing SINR constraint $\gamma_k^r[n] \geqslant \Gamma$, it is sufficient to ensure that this maximum eigenvalue is no less than Γ. Let $\lambda_{j,k}^{\max}[n]$ denote the largest eigenvalue of $\mathbf{F}_{j,k}^{-1/2}[n]\mathbf{E}_{j,k}[n]\mathbf{F}_{j,k}^{-1/2}[n]$. The problem (P5) can then be equivalently reformulated as

$$\begin{aligned}(\text{P6}): \quad & \max_{\{\mathbf{u}_{j,k}[n]\}} \sum_{n\in\mathcal{N}} R[n] \\ \text{s.t.} \quad & \sum_{j\in\mathcal{M}} \lambda_{j,k}^{\max}[n] \geqslant \Gamma. \end{aligned} \tag{40}$$

The optimal receive filter $\mathbf{u}_{j,k}^*[n]$ is thus obtained as the eigenvector associated with the largest eigenvalue of the matrix $\mathbf{F}_{j,k}^{-1/2}[n]\mathbf{E}_{j,k}[n]\mathbf{F}_{j,k}^{-1/2}[n]$. This solution ensures that the sensing SINR is maximized under the given constraint and that $\mathbf{u}_{j,k}[n]$ is aligned with the most favorable eigenmode of the effective sensing channel [16].

3.4 UAV trajectory optimization

In this section, our goal is to optimize the UAV trajectory design $\mathbf{q}_k[n]$, while keeping the beamforming vectors $\mathbf{W}_{m,k}^c[n]$ and $\mathbf{W}_{m,k}^r[n]$, as well as the receive filter $\mathbf{u}_{j,k}[n]$, fixed. The optimization problem is formally expressed as

$$\begin{aligned}(\text{P7}): & \max_{\{\mathbf{q}_k[n]\}} \sum_{n\in\mathcal{N}} R[n] \\ & \text{s.t. (21b), (21d), (21e), (21f), (21g).}\end{aligned}$$

Constraints (21d) and (21e) ensure that the UAVs adhere to the specified initial and final positions, constraint (21f) imposes a maximum velocity limit on UAV movement, and constraint (21g) enforces collision avoidance between UAVs. However, constraint (21g) is nonconvex, making direct optimization challenging. The trajectory variable $\mathbf{q}_k[n]$ appears in $\theta_{m,k}[n]$, which directly impacts the achievable rate $R_k[n]$. Therefore, it is necessary to process the nonconvexity of (21g) and reformulate $R_k[n]$ to facilitate optimization.

To handle this, we first apply the SCA method to approximate the non-convex constraint (21g). In the f-th iteration, the UAV trajectory variable $\mathbf{q}_k[n]$ is represented as $\mathbf{q}_k^{(f)}[n]$. Using the first-order Taylor expansion around $\mathbf{q}_k^{(f)}[n]$, the original constraint (20g) is approximated as

$$-\|\mathbf{q}_j^{(f)}[n] - \mathbf{q}_i^{(f)}[n]\|^2 + 2(\mathbf{q}_j^{(f)}[n] - \mathbf{q}_i^{(f)}[n])^{\mathrm{T}}(\mathbf{q}_j[n] - \mathbf{q}_i[n]) \geqslant D_{\min}^2 - (H_j - H_i)^2. \tag{41}$$

This reformulation transforms the original non-convex constraint into a convex one, making it easier to solve by using convex optimization techniques.

Next, we reformulate the achievable communication rate $R_k[n]$ in the objective function to facilitate subsequent derivations. Let $[\mathbf{W}_{m,i}^c[n]]p,q$ and $[\mathbf{W}_{m,i}^r[n]]p,q$ denote the (p,q)-th entries of the beamforming matrices $\mathbf{W}_{m,i}^c[n]$ and $\mathbf{W}_{m,i}^r[n]$, respectively, and their phases are defined as $\theta_{p,q}^c$ and $\theta_{p,q}^r$.

Based on these notations, $R_k[n]$ can be rewritten in a more tractable form, enabling precise handling of its non-linear components. This reformulation lays the foundation for iterative optimization via convex approximation techniques. The resulting relationship is given by

$$\begin{aligned}R_k[n] = & \log_2\left(\sum_{m\in\mathcal{M}}\sum_{i\in\mathcal{K}_{cs}} \eta_{m,i,k}[n] + \sum_{m\in\mathcal{M}}\sum_{i\in\mathcal{K}} \mu_{m,i,k}[n] + \sum_{m\in\mathcal{M}} \frac{\sigma^2}{\kappa}(\|\mathbf{q}_k[n] - \mathbf{v}_m\|^2 + H_k^2)\right) \\ & - \log_2\left(\sum_{m\in\mathcal{M}}\sum_{i\in\mathcal{K}_{cs}\setminus k} \eta_{m,i,k}[n] + \sum_{m\in\mathcal{M}}\sum_{i\in\mathcal{K}} \mu_{m,i,k}[n] + \sum_{m\in\mathcal{M}} \frac{\sigma^2}{\kappa}(\|\mathbf{q}_k[n] - \mathbf{v}_m\|^2 + H_k^2)\right),\end{aligned} \tag{42}$$

where $\eta_{m,i,k}[n]$ and $\mu_{m,i,k}[n]$ are expressed as

$$\eta_{m,i,k}[n] = \sum_{z=1}^{L} [\mathbf{W}_{m,i}^c[n]]_{z,z} + 2\sum_{p=1}^{L}\sum_{q=p+1}^{L} |[\mathbf{W}_{m,i}^c[n]]_{p,q}| \times \cos\left(\theta_{p,q}^c + 2\pi\frac{d}{\lambda}(q-p)\frac{H_k}{\sqrt{\|\mathbf{q}_k[n] - \mathbf{v}_m\|^2 + H_k^2}}\right), \tag{43}$$

and

$$\mu_{m,i,k}[n] = \sum_{z=1}^{L} [\mathbf{W}_{m,i}^r[n]]_{z,z} + 2\sum_{p=1}^{L}\sum_{q=p+1}^{L} |[\mathbf{W}_{m,i}^c[n]]_{p,q}| \times \cos\left(\theta_{p,q}^r + 2\pi\frac{d}{\lambda}(q-p)\frac{H_k}{\sqrt{\|\mathbf{q}_k[n] - \mathbf{v}_m\|^2 + H_k^2}}\right). \tag{44}$$

Subsequently, we approximate (42) by using the first-order Taylor expansion in iteration f as

$$R_k[n] \approx \tilde{R}_k^{(f)}[n] = c_k^{(f)}[n] + \mathbf{d}_k^{(f)T}[n](\mathbf{q}_k[n] - \mathbf{q}_k^{(f)}[n]), \tag{45}$$

where

$$\begin{aligned} c_k^{(f)}[n] = &\log_2\left(\sum_{m\in\mathcal{M}}\sum_{i\in\mathcal{K}_{cs}}\eta_{m,i,k}^{(f)}[n] + \sum_{m\in\mathcal{M}}\sum_{i\in\mathcal{K}}\mu_{m,i,k}^{(f)}[n] + \sum_{m\in\mathcal{M}}\frac{\sigma^2}{\kappa}(\|\mathbf{q}_k^{(f)}[n]-\mathbf{v}_m\|^2 + H_k^2)\right) \\ &- \log_2\left(\sum_{m\in\mathcal{M}}\sum_{i\in\mathcal{K}_{cs}\backslash k}\eta_{m,i,k}^{(f)}[n] + \sum_{m\in\mathcal{M}}\sum_{i\in\mathcal{K}}\mu_{m,i,k}^{(f)}[n] + \sum_{m\in\mathcal{M}}\frac{\sigma^2}{\kappa}(\|\mathbf{q}_k^{(f)}[n]-\mathbf{v}_m\|^2 + H_k^2)\right), \end{aligned} \tag{46}$$

$$\begin{aligned} \mathbf{d}_k^{(f)}[n] = &\frac{\log_2 e}{\phi_k[n]}\left(\sum_{m\in\mathcal{M}}\sum_{i\in\mathcal{K}_{cs}}\gamma_{m,i,k}^{(f)}[n] + \sum_{m\in\mathcal{M}}\sum_{i\in\mathcal{K}}\omega_{m,i,k}^{(f)}[n](\mathbf{q}_k^{(f)}[n]-\mathbf{v}_m)\right) \\ &- \frac{\log_2 e}{\psi_k[n]}\left(\sum_{m\in\mathcal{M}}\sum_{i\in\mathcal{K}_{cs}\backslash k}\gamma_{m,i,k}^{(f)}[n] + \sum_{m\in\mathcal{M}}\sum_{i\in\mathcal{K}}\omega_{m,i,k}^{(f)}[n](\mathbf{q}_k^{(f)}[n]-\mathbf{v}_m)\right), \end{aligned} \tag{47}$$

where $\gamma_{m,i,k}^{(f)}[n]$, $\omega_{m,i,k}^{(f)}[n]$, $\phi_k[n]$ and $\psi_k[n]$ are defined respectively as follows:

$$\gamma_{m,i,k}^{(f)}[n] = \sum_{p=1}^{L}\sum_{q=p+1}^{L} 4\pi|[\mathbf{W}_{m,i}^c[n]]_{p,q}| \times \sin\left(\theta_{p,q}^c + 2\pi\frac{d}{\lambda}(q-p)\frac{H_k}{\sqrt{\|\mathbf{q}_k^{(f)}[n]-\mathbf{v}_m\|^2+H_k^2}}\right)\cdot\frac{dH_k(q-p)}{\lambda(\|\mathbf{q}_k^{(f)}[n]-\mathbf{v}_m\|^2+H_k^2)^{\frac{3}{2}}}, \tag{48}$$

$$\omega_{m,i,k}^{(f)}[n] = \sum_{p=1}^{L}\sum_{q=p+1}^{L} 4\pi|[\mathbf{W}_{m,i}^r[n]]_{p,q}| \times \sin\left(\theta_{p,q}^r + 2\pi\frac{d}{\lambda}(q-p)\frac{H_k}{\sqrt{\|\mathbf{q}_k^{(f)}[n]-\mathbf{v}_m\|^2+H_k^2}}\right)\cdot\frac{dH_k(q-p)}{\lambda(\|\mathbf{q}_k^{(f)}[n]-\mathbf{v}_m\|^2+H_k^2)^{\frac{3}{2}}}, \tag{49}$$

$$\phi_k[n] = \sum_{m\in\mathcal{M}}\sum_{i\in\mathcal{K}_{cs}}\eta_{m,i,k}^{(f)}[n] + \sum_{m\in\mathcal{M}}\sum_{i\in\mathcal{K}}\mu_{m,i,k}^{(f)}[n] + \sum_{m\in\mathcal{M}}\frac{\sigma^2}{\kappa}(\|\mathbf{q}_k^{(f)}[n]-\mathbf{v}_m\|^2 + H_k^2), \tag{50}$$

$$\psi_k[n] = \sum_{m\in\mathcal{M}}\sum_{i\in\mathcal{K}_{cs}\backslash k}\eta_{m,i,k}^{(f)}[n] + \sum_{m\in\mathcal{M}}\sum_{i\in\mathcal{K}}\mu_{m,i,k}^{(f)}[n] + \sum_{m\in\mathcal{M}}\frac{\sigma^2}{\kappa}(\|\mathbf{q}_k^{(f)}[n]-\mathbf{v}_m\|^2 + H_k^2). \tag{51}$$

Similarly, we reformulate constraint (21b) in terms of $\mathbf{q}_k[n]$ and ensure convexity.

Let $\tilde{\mathbf{A}}_{m,k}[n] = \mathbf{A}_{m,k}^{\mathrm{H}}[n]\mathbf{u}_{m,k}[n]\mathbf{u}_{m,k}^{\mathrm{H}}[n]\mathbf{A}_{m,k}[n]$, so as to $\tilde{\mathbf{H}}_{\mathrm{SI},j}$ and $\tilde{\mathbf{G}}_{i,j}$. Then Eq. (24) can be reformulated as

$$\gamma_k^r[n] = \frac{\sigma_t^2\sum\limits_{j\in\mathcal{M}}\mathrm{tr}(\tilde{\mathbf{A}}_{j,k}[n]\mathbf{X}_j[n])}{\sum\limits_{j\in\mathcal{M}}[\mathrm{tr}(\tilde{\mathbf{H}}_{\mathrm{SI},j}\mathbf{X}_j[n]) + \mathrm{tr}(\tilde{\mathbf{G}}_{i,j}\mathbf{X}_j[n]) + \sigma_r^2\mathbf{I}_L + \sigma_t^2\sum\limits_{l\neq k,l\in\mathcal{K}}\mathrm{tr}(\tilde{\mathbf{A}}_{j,k}[n]\mathbf{X}_j[n])]}. \tag{52}$$

Let $\mathbf{u}_{m,k}[n] = [\alpha_1, \alpha_2, ..., \alpha_L]^{\mathrm{T}}$, $\tilde{\mathbf{a}}_{m,k}[n] = \mathbf{A}_{m,k}^{\mathrm{H}}[n]\cdot\mathbf{u}_{m,k}[n] = \mathbf{A}_{m,k}[n]\cdot\mathbf{u}_{m,k}[n]$. Then we have $[\tilde{\mathbf{a}}_{m,k}[n]]_i = \sum_{q=1}^{L}\alpha_q\cdot e^{j2\pi\frac{d}{\lambda}(i-q)\cos\theta_{m,k}[n]}$, $1\leqslant k\leqslant L$. Since $\tilde{\mathbf{A}}_{m,k}[n] = \tilde{\mathbf{a}}_{m,k}[n]\cdot\tilde{\mathbf{a}}_{m,k}^{\mathrm{H}}[n]$, $[\tilde{\mathbf{A}}_{m,k}[n]]_{p,q}$ can be expressed as

$$\begin{aligned} [\tilde{\mathbf{A}}_{m,k}[n]]_{p,q} &= \left(\sum_{s=1}^{L}\alpha_s e^{j2\pi\frac{d}{\lambda}(p-s)\cos\theta_{m,k}[n]}\right)\cdot\left(\sum_{t=1}^{L}\alpha_t^* e^{-j2\pi\frac{d}{\lambda}(q-t)\cos\theta_{m,k}[n]}\right) \\ &= \sum_{s=1}^{L}\sum_{t=1}^{L}\alpha_m\alpha_n^* e^{j2\pi\frac{d}{\lambda}[p-q-(s-t)]\cos\theta_{m,k}[n]}. \end{aligned} \tag{53}$$

Next, we approximate $\mathrm{tr}(\tilde{\mathbf{A}}_{j,k}[n]\mathbf{X}_j[n])$ by using the first-order Taylor expansion in iteration f as

$$\mathrm{tr}(\tilde{\mathbf{A}}_{j,k}[n]\mathbf{X}_j[n]) = h_{j,k}^{(f)}[n] + \boldsymbol{i}_{j,k}^{(f)}[n](\mathbf{q}_k[n] - \mathbf{q}_k^{(f)}[n]), \tag{54}$$

where

$$h_{j,k}^{(f)}[n] = \sum_{s=1}^{L}\sum_{t=1}^{L}\alpha_s\alpha_t^* \cdot \left[\sum_{z=1}^{L}[\mathbf{X}_j[n]]_{z,z} + 2\sum_{p=1}^{L}\sum_{q=p+1}^{L}|[\mathbf{X}_j[n]]_{z,z}| \times \cos\left(\theta_{p,q}^x + 2\pi\frac{d}{\lambda}\frac{(p-q+t-s)H_k}{\sqrt{\|\mathbf{q}_k^{(f)}[n]-\mathbf{v}_m\|^2+H_k^2}}\right)\right], \tag{55}$$

$$\boldsymbol{i}_{j,k}^{(f)}[n] = \sum_{s=1}^{L}\sum_{t=1}^{L}\alpha_s\alpha_t^* \cdot \left[\sum_{p=1}^{L}\sum_{q=p+1}^{L}4\pi|\mathbf{X}_{j,k}[n]\sin\left(\theta_{p,q}^x + \frac{2\pi d(p-q+t-s)H_k}{\sqrt{\|\mathbf{q}_k^{(f)}[n]-\mathbf{v}_m\|^2+H_k^2}}\right) \times \frac{d(p-q+t-s)H_k}{\lambda(\|\mathbf{q}_k^{(f)}[n]-\mathbf{v}_m\|^2+H_k^2)^{\frac{3}{2}}}\right], \tag{56}$$

in which $\theta_{p,q}^x$ represents the phase of the entries.

By bringing the formula (54) into (52), the constraint (21b) can be transformed into the form of the constraint (57). It is clear that the inequality constraint is linear with respect to $\mathbf{q}_k[n]$, and therefore the constraint is convex.

$$\begin{aligned}&\sigma_t^2 \sum_{j\in\mathcal{M}}[h_{j,k}^{(f)}[n] + \boldsymbol{i}_{j,k}^{(f)}[n](\mathbf{q}_k[n] - \mathbf{q}_k^{(f)}[n])]\\ \geqslant&\Gamma \cdot \sum_{j\in\mathcal{M}}\{\mathrm{tr}(\tilde{\mathbf{H}}_{\mathrm{SI},j}\mathbf{X}_j[n]) + \mathrm{tr}(\tilde{\mathbf{G}}_{i,j}\mathbf{X}_j[n]) + \sigma_r^2\mathbf{I}_L + \sigma_t^2\sum_{l\neq k, l\in\mathcal{K}}[h_{j,k}^{(f)}[n] + \boldsymbol{i}_{j,k}^{(f)}[n](\mathbf{q}_k[n] - \mathbf{q}_k^{(f)}[n])]\}.\end{aligned} \tag{57}$$

To address the non-convexity of the objective function in (42), we reformulate it into a linearized form, as presented in (45). This reformulation simplifies the problem and makes it suitable for convex optimization techniques. However, to ensure the accuracy of the linear approximation at each iterative step, a mechanism called the trust region constraint [11] is introduced. The trust region constraint is mathematically expressed as

$$\|\mathbf{q}_k^{(f)}[n] - \mathbf{q}_k^{(f-1)}[n]\| \leqslant \varepsilon^{(f)}, \quad \forall k \in \mathcal{K},\, n \in \mathcal{N}, \tag{58}$$

where $\varepsilon^{(f)}$ represents the radius of the trust region in the f-th iteration. This constraint ensures that the trajectory update between successive iterations remains within a bounded region, maintaining the validity of the first-order approximation.

Incorporating the trust region and approximated terms, problem (P7) is reformulated as the convex problem (P8) for iteration f, expressed as

$$\begin{aligned}(\mathrm{P8}): &\max_{\{\mathbf{q}_k[n]\}} \sum_{n\in\mathcal{N}}\sum_{k\in\mathcal{K}}\omega_k\tilde{R}_k^{(f)}[n]\\ &\text{s.t.} \quad (21\text{b}),\ (21\text{e}),\ (21\text{f}),\ (41),\ (57),\ (58).\end{aligned}$$

This convex approximation problem can be efficiently solved using numerical tools such as CVX, a solver designed for convex optimization. The specific solution algorithm for problem (P8) is as shown in Algorithm 1.

Algorithm 1 Trajectory optimization algorithm for problem (P8).

Initialize: UAV trajectory $\{\hat{\mathbf{q}}^{(0)}[n]\}$, trust region $\psi^{(0)}$, outer iteration index $f = 1$;
repeat
  Let $l = 1$; set $\{\mathbf{q}^{(l-1)}[n]\} = \{\hat{\mathbf{q}}^{(f-1)}[n]\}$;
  repeat
    Solve problem (P8) under local point $\{\mathbf{q}^{(l-1)}[n], \mathbf{W}_k^{(f)}[n], \mathbf{R}_s^{(f)}[n]\}$ to obtain $\{\mathbf{q}^{(l)*}[n]\}$;
    if objective value of problem (P8) increases **then**
      $\{\mathbf{q}^{(l)}[n]\} = \{\mathbf{q}^{(l)*}[n]\}$, $l \leftarrow l + 1$;
    else
      Update trust region: $\psi^{(l)} = \psi^{(l)}/2$;
    end if
  until $\psi^{(l)} < \hat{\varepsilon}$;
  Update UAV trajectory: $\{\hat{\mathbf{q}}^{(f)}[n]\} = \{\mathbf{q}^{(l)}[n]\}$, $f \leftarrow f + 1$;
until the objective value converges within tolerance $\bar{\varepsilon}$.

The computational complexity of the proposed alternating optimization algorithm is analyzed by examining the three subproblems solved in each outer iteration. The transmit beamforming optimization (P3) is addressed by solving a semidefinite program (SDP) via the SDR technique. The receive filter optimization (P5) requires computing the dominant eigenvector of a matrix, which is a standard linear algebra operation. Similarly, the UAV trajectory optimization (P7) is transformed into a convex problem. It is well-established that standard convex optimization problems, such as SDPs, and eigenvector computations can be solved efficiently with a complexity

that is a polynomial function of the problem size. Among these steps, solving the SDP for beamforming typically constitutes the main computational bottleneck. Since each of the core subproblems is solvable in polynomial time, the overall proposed algorithm has a polynomial-time complexity, ensuring its computational tractability for moderately sized networks.

In summary, the proposed algorithm for solving problem (P7) operates iteratively by solving a sequence of convex subproblems, where each subproblem refines the solution using the trust region and linearized approximations. As established by our analysis, since only problems with polynomial-time complexity are solved in each iteration, the algorithm can be efficiently implemented and is expected to achieve fast convergence in wireless networks with a moderate number of users. The methods for the subproblems (P3), (P5), and (P7) converge by either finding the optimal solution or by successive refinements of the approximations. As a result, the overall AO technique is guaranteed to converge to a locally optimal solution for the joint UAV trajectory design and beamforming optimization problem.

4 Numerical results

This section presents numerical results to evaluate the performance of the proposed design. In the simulation, we consider $K_{cs} = 2$ ISAC UAVs, $K_s = 2$ sensing UAVs, and $M = 4$ BSs located near the UAV trajectories. Each BS is equipped with $L = 8$ antennas with spacing $d = \lambda/2$. The initial and final positions of the ISAC UAVs are set as $\mathbf{q}_1^{\mathrm{I}} = [50\,\mathrm{m}, 150\,\mathrm{m}]$, $\mathbf{q}_1^{\mathrm{F}} = [550\,\mathrm{m}, 150\,\mathrm{m}]$, and $\mathbf{q}_2^{\mathrm{I}} = [50\,\mathrm{m}, 450\,\mathrm{m}]$, $\mathbf{q}_2^{\mathrm{F}} = [550\,\mathrm{m}, 450\,\mathrm{m}]$. For the sensing UAVs, we set $\mathbf{q}_3^{\mathrm{I}} = [50\,\mathrm{m}, 250\,\mathrm{m}]$, $\mathbf{q}_3^{\mathrm{F}} = [550\,\mathrm{m}, 250\,\mathrm{m}]$, and $\mathbf{q}_4^{\mathrm{I}} = [50\,\mathrm{m}, 350\,\mathrm{m}]$, $\mathbf{q}_4^{\mathrm{F}} = [550\,\mathrm{m}, 350\,\mathrm{m}]$. The UAV altitude is fixed at $H_k = 100\,\mathrm{m}$, the time horizon T is divided into $N = 30$ slots, and the maximum UAV speed is $V_{\max} = 20\,\mathrm{m/s}$. A larger choice of N typically yields finer time quantization and consequently improved performance. However, it also incurs a higher computational burden. Hence, the selection of N inherently involves a fundamental trade-off between computational complexity and system performance. Each BS has a maximum transmit power of $P_{\max} = 10\,\mathrm{W}$. This power level is representative of small-cell base stations often considered for dense network deployments supporting applications like the low-altitude economy. The reference channel power gain at $d_0 = 1\,\mathrm{m}$ is set to $-45\,\mathrm{dB}$, and the noise power at UAVs is $-100\,\mathrm{dBW}$. The RCS of each UAV is modeled as $\xi_{j,l} \sim \mathcal{CN}(0, 1)$. The self-interference coefficient is $\zeta_{j,l} = -110\,\mathrm{dB}$, which represents a practical scenario with highly effective self-interference cancellation (SIC) technologies assumed at the BSs. The inter-BS interference coefficient is $\alpha_{j,l} = -30\,\mathrm{dB}$, a commonly used value to model the inter-site signal isolation in moderately dense deployments. All weight parameters are set to $\omega_k = 1$, which establishes a fair baseline for performance comparison, allowing the analysis to focus on the fundamental gains from the joint optimization of trajectory and beamforming. This ensures that observed performance improvements are due to efficient resource management rather than user prioritization. Conversely, assigning non-uniform weights would direct the system to prioritize UAVs with higher importance. The algorithm would allocate more resources—such as transmit power or a more favorable flight path—to these UAVs to enhance their communication rates, potentially at the expense of lower-priority ones. Our proposed framework is fully capable of supporting such service differentiation.

For performance comparison, the following benchmark schemes are considered.

(1) Optimized beamforming with a uniform straight-line trajectory: In this scenario, UAV trajectories are fixed as straight lines from initial to final positions, with constant speed $V_k = \frac{1}{N}\|\mathbf{q}_k^{\mathrm{I}} - \mathbf{q}_k^{\mathrm{F}}\|$. Given this non-adaptive trajectory, the beamforming matrices $\{\mathbf{W}_{m,i}^c[n]\}$ and $\{\mathbf{W}_{m,i}^r[n]\}$ are optimized by solving problem (P4) to enhance communication performance during flight.

(2) Optimized beamforming and straight-line trajectory with optimized speed: This benchmark extends the previous one by allowing UAVs to adjust their speeds along fixed straight-line paths. The speeds are optimized to improve communication by enabling UAVs to spend more time in favorable locations. Problem (P2) is solved to jointly optimize the beamforming matrices and UAV positions $\{\mathbf{q}_k[n]\}$, under the constraint of linear trajectories with variable speeds.

(3) Optimized trajectory, not beamforming: Here, UAV trajectories are optimized while beamforming follows an equal power allocation strategy: $\mathbf{W}_{m,i}^c[n] = \frac{p_{j,l}^c[n]}{L}\mathbf{I}_L$, $\mathbf{W}_{m,i}^r[n] = \frac{p_{j,l}^r[n]}{L}\mathbf{I}_L$, where $p_{j,l}^c[n]$ and $p_{j,l}^r[n]$ are constrained by $\sum_{i\in\mathcal{K}_{cs}} p_{j,l}^c[n] + \sum_{i\in\mathcal{K}} p_{j,l}^r[n] \leqslant P_{\max}$. UAV trajectories $\{\mathbf{q}_k[n]\}$ are then optimized by solving problem (P8) with fixed beamforming, aiming to improve communication despite non-adaptive transmission.

(4) Dynamic best-server selection with joint optimization: In this non-cooperative benchmark, each UAV k is dynamically served by only one ground BS at each time slot n. This exclusive association is modeled using a binary variable $a_{m,k}^d[n]$, where $a_{m,k}^d[n] = 1$ if BS m is selected to serve UAV k at slot n, and $a_{m,k}^d[n] = 0$ otherwise. This selection satisfies the constraint $\sum_{m\in\mathcal{M}} a_{m,k}^d[n] = 1$ for each UAV. The serving BS is chosen as the

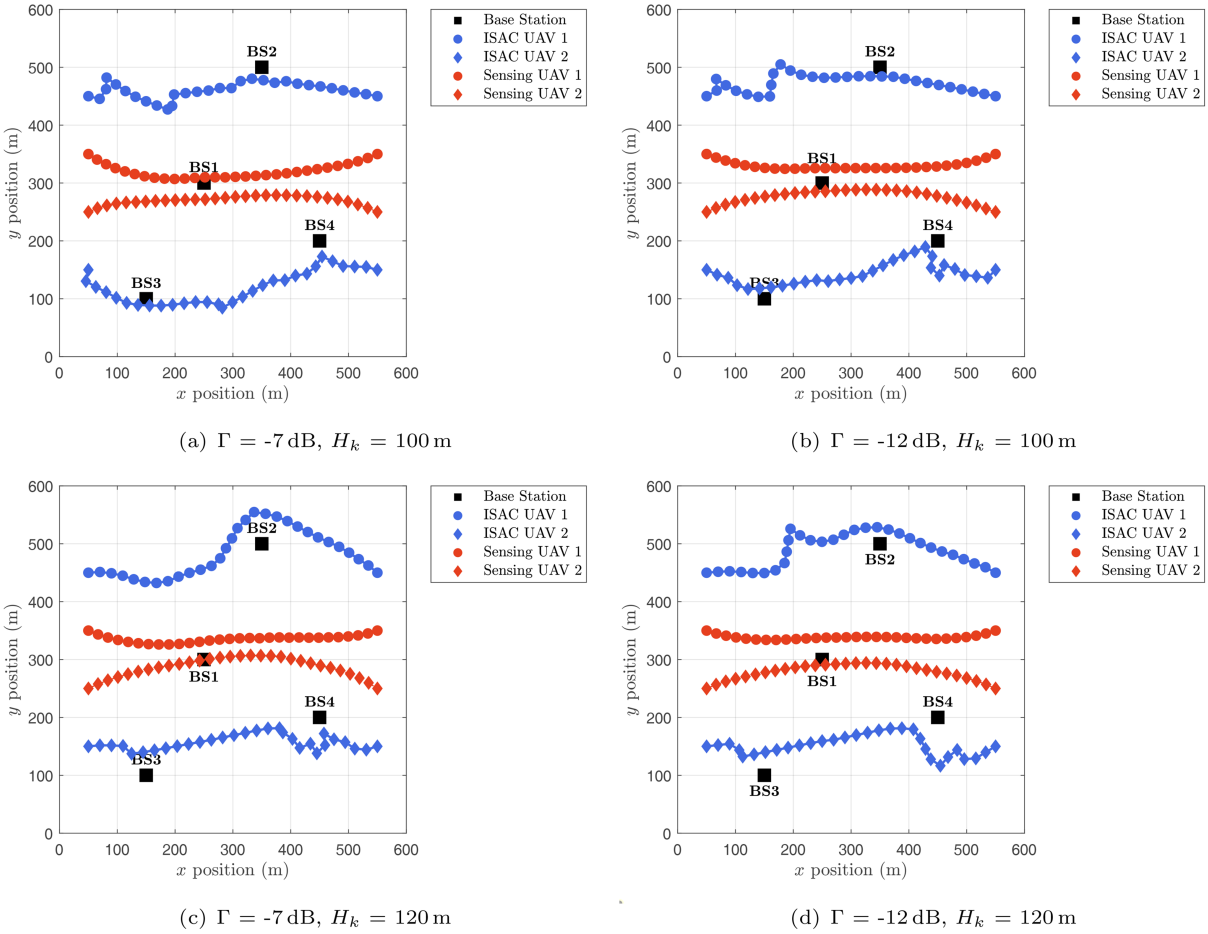

(a) Γ = -7 dB, H_k = 100 m

(b) Γ = -12 dB, H_k = 100 m

(c) Γ = -7 dB, H_k = 120 m

(d) Γ = -12 dB, H_k = 120 m

Figure 2 (Color online) Optimal UAV trajectories under different altitudes and sensing thresholds.

one providing the strongest instantaneous channel link, meaning $a^d_{m,k}[n]$ is set to 1 for the BS m that maximizes $\|h_{m,k}[n]\|^2$. The UAV trajectories and transmit beamforming are then jointly optimized. The communication rate for UAV k is calculated based on the signal from its single serving BS, while treating signals from all other BSs as interference.

The first three benchmarks are designed to perform an ablation study, isolating the performance gains from each key component of the joint optimization framework. They respectively demonstrated the significance and advantages of optimizing different variables. In contrast, the fourth benchmark, dynamic best-server selection, represents a mainstream and highly effective non-cooperative strategy, often considered a state-of-the-art (SOTA) approach in multi-cell UAV networks [3, 41]. Therefore, a direct comparison against this SOTA benchmark is necessary to rigorously validate the superiority of our proposed cooperative scheme, highlighting the significant advantages offered by cooperative transmission and joint design over current advanced, non-cooperative techniques.

Through analyzing the optimized UAV trajectories shown in Figure 2, we can explore the impact of different sensing SINR thresholds Γ and UAV flight altitudes H_k on trajectory optimization.

The sensing SINR threshold significantly affects UAV trajectories, as shown by comparing Figures 2(a) and (b) at $H_k = 100\,\text{m}$, and Figures 2(c) and (d) at $H_k = 120\,\text{m}$. In both cases, increasing the threshold from $\Gamma = -12\,\text{dB}$ to $\Gamma = -7\,\text{dB}$ causes the trajectories to become more concentrated and closer to the BSs. This is because a higher sensing requirement compels UAVs to fly in regions where BSs can receive stronger echo signals, enhancing sensing performance. In contrast, a lower threshold permits greater trajectory flexibility, allowing a more balanced trade-off between communication and sensing. Thus, higher thresholds lead to sensing-driven path planning, while lower thresholds offer more freedom to optimize communication.

UAV altitude also plays a critical role in trajectory optimization. This is evident by comparing Figures 2(a) and (c) for $\Gamma = -7\,\text{dB}$, and Figures 2(b) and (d) for $\Gamma = -12\,\text{dB}$. As altitude increases from $H_k = 100\,\text{m}$ to $H_k = 120\,\text{m}$, trajectory distributions change notably. Higher altitudes introduce greater propagation loss for sensing echoes and degrade communication link quality due to longer distances. Conversely, lower altitudes yield better channel

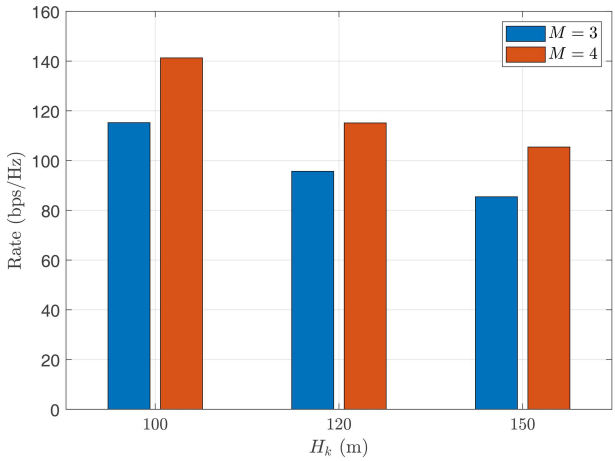

Figure 3 (Color online) Weighted sum rate versus UAV flight altitude H_k under different numbers of BSs ($\Gamma = -12$ dB).

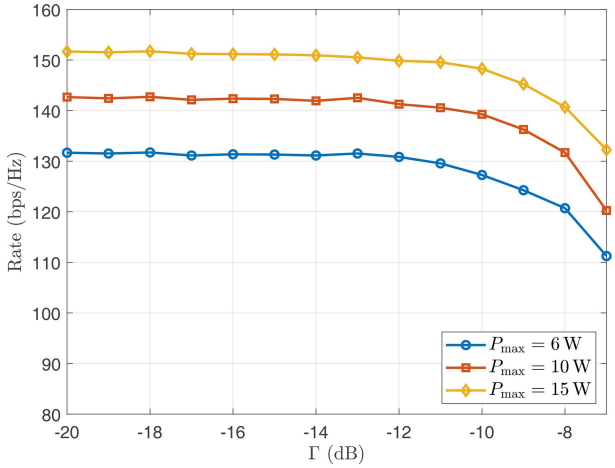

Figure 4 (Color online) Weighted sum rate versus sensing SINR threshold Γ under different BS transmit power limits $P_{\max}$.

conditions, enabling more effective trajectory planning. These results highlight the importance of jointly optimizing altitude and trajectory to balance sensing and communication performance based on specific mission requirements.

Figure 3 illustrates the impact of UAV altitude on the weighted sum rate under varying BS densities, with the sensing SINR threshold fixed at $\Gamma = -12$ dB. As altitude increases, the communication rate declines due to increased path loss and degraded channel quality between UAVs and BSs. Additionally, deploying more BSs significantly enhances system performance. Specifically, the three-BS configuration is derived by removing one BS from the original four-BS layout. Across all altitudes, the four-BS setup consistently outperforms the three-BS case, benefiting from greater spatial diversity and improved beamforming flexibility. Although additional BSs may introduce interference, coordinated beamforming with enhanced spatial resolution effectively mitigates it. These results underscore the importance of jointly optimizing UAV altitude and BS deployment to improve ISAC performance.

Figure 4 shows how the weighted sum rate varies with the sensing SINR threshold Γ under different BS power limits ($P_{\max} = 6$ W, 10 W, and 15 W). As Γ increases, stricter sensing requirements reduce the degrees of freedom available for communication, leading to a noticeable decline in rate. However, increasing the BS transmit power alleviates this trade-off by providing more resources to support both tasks simultaneously. Higher power budgets help maintain communication performance even under tight sensing constraints. These findings suggest that appropriately increasing BS power enhances system robustness and elevates the achievable performance ceiling of ISAC systems.

Figure 5 illustrates the impact of various trajectories and beamforming optimization schemes on the communication rate under different sensing SINR thresholds Γ. As Γ increases, all schemes exhibit a rate decline due to the trade-off between sensing and communication, where more resources are required to satisfy sensing constraints, those available for communication. Among the schemes, the proposed joint trajectory and cooperative beamforming optimization consistently achieve the highest rates across all Γ values, demonstrating strong adaptability and performance. Following this is the dynamic best-server selection scheme, which serves as a powerful non-cooperative baseline. Although it intelligently adapts by selecting the best single server at each moment, the noticeable performance gap highlights the clear superiority of our proposed cooperative approach. This gain is attributed to the ability of multiple BSs to perform coordinated multi-point transmission, which not only enhances the desired signal but also actively mitigates inter-BS interference, a capability that single-server strategies inherently lack. The scheme with a fixed straight-line trajectory but optimized speed performs reasonably well but remains inferior to the fully optimized trajectory case, indicating that speed control alone offers limited benefit compared to full spatial trajectory design. In contrast, optimizing only beamforming with a fixed trajectory and constant speed yields substantially lower but stable rate curves. Lastly, the scheme with optimized trajectory but fixed, non-adaptive beamforming becomes infeasible at higher Γ values, resulting in a truncated curve and highlighting the essential role of beamforming in maintaining sensing feasibility. Overall, the results confirm that joint optimization of trajectory and beamforming is key to maximizing communication performance under varying sensing demands.

The proposed framework is particularly applicable to practical low-altitude scenarios where LoS links are dominant, such as over open or suburban areas for applications like precision agriculture and infrastructure inspection.

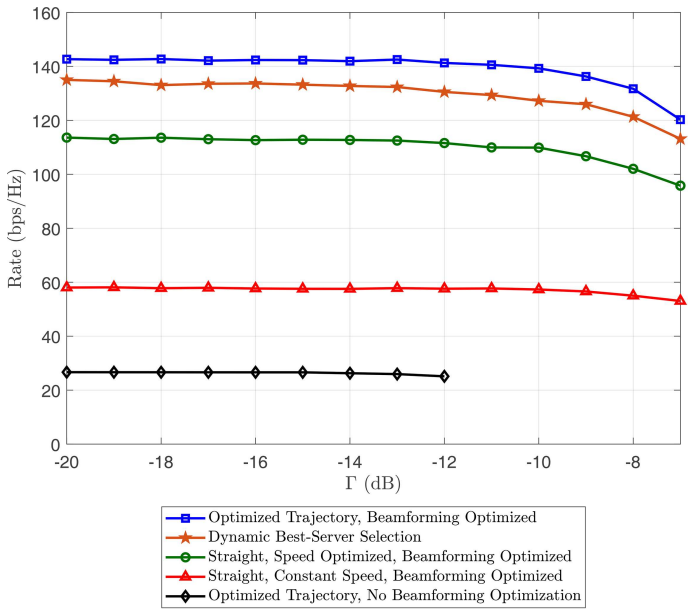

Figure 5 (Color online) Weighted sum rate versus sensing SINR threshold Γ under different trajectory and beamforming optimization strategies.

The focus on an LoS channel model is justified by the common condition in many air-to-ground deployments where the UAV's altitude provides a clear, stable direct path to the ground base stations, rendering NLoS effects negligible. This LoS assumption is not only practical for these scenarios but also crucial for analytical tractability. Introducing statistical NLoS components would obscure this direct relationship and significantly increase the complexity of the optimization problem. While NLoS components can become more prominent in dense urban canyons, our approach provides a crucial and robust foundation for these widespread, LoS-dominant use cases.

Further investigation into the scalability of the proposed framework is a crucial aspect for practical deployment. The scale of the optimization problem is primarily determined by the number of base stations, UAVs, antennas per BS, and time slots. The number of optimization variables, particularly the semidefinite beamforming matrices, grows with these factors, directly impacting the computational load. As identified in our analysis, the main computational bottleneck is the SDP used for beamforming optimization. The complexity of solving this SDP is a high-order polynomial function of the system dimensions, which is why the proposed algorithm is most tractable for the moderately sized networks considered in this work. To extend the framework's applicability to large-scale systems, future research should focus on mitigating this complexity. Promising directions include the development of more scalable solutions, such as distributed optimization techniques that decompose the central problem, or machine learning-based approaches that can learn to approximate the optimal policy with significantly lower real-time computational overhead.

5 Conclusion

This paper proposed a joint trajectory and cooperative beamforming framework for a UAV-enabled ISAC system. We formulated a non-convex problem to maximize the weighted sum rate under sensing SINR constraints and solved it using an efficient alternating optimization algorithm based on SDR and SCA. Simulation results demonstrated that our joint cooperative design outperforms non-cooperative benchmark schemes, delivering higher communication throughput while ensuring robust sensing performance. The findings highlight the critical role of trajectory adaptation in balancing sensing and communication trade-offs, providing a robust baseline for future extensions toward large-scale and complex environments.

Acknowledgements This work was supported by National Natural Science Foundation of China (Grant No. 62350710796), Jiangsu Outstanding Youth Fund (Grant No. BK20240071), Scientific Research Innovation Capability Support Project for Young Faculty (Grant Nos. 3204002501C3, U40), and Fundamental Research Funds for the Central Universities (Grant No. 2242025K20001).

References

1 Zhang Y, Shan H, Zhou Y, et al. Cooperative beamforming design for anti-UAV ISAC systems. IEEE Trans Wireless Commun, 2025, 24: 2249–2264
2 Meng K, Wu Q, Xu J, et al. UAV-enabled integrated sensing and communication: opportunities and challenges. IEEE Wireless Commun, 2024, 31: 97–104

3 Cheng G, Song X, Lyu Z, et al. Networked ISAC for low-altitude economy: transmit beamforming and UAV trajectory design. In: Proceedings of IEEE/CIC International Conference on Communications in China (ICCC), 2024. 78–83
4 Long H, Chen M, Yang Z, et al. Joint trajectory and passive beamforming design for secure UAV networks with RIS. In: Proceedings of IEEE GlobeCom Workshops (GCWkshps), 2020. 1–6
5 Liu J Q, Yang P, Jiang K, et al. OFDM-structure based waveform designs for integrated sensing and communication. Sci China Inf Sci, 2025, 68: 150306
6 Xu Y, Li Y, Zhang J A, et al. Joint beamforming for RIS-assisted integrated sensing and communication systems. IEEE Trans Commun, 2024, 72: 2232–2246
7 Liu G Y, Xi R Y, Jiang T, et al. Feasibility study of cooperative sensing: radar cross section, synchronization, cooperative cluster, performance and prototype. Sci China Inf Sci, 2025, 68: 150302
8 Zeng F, Liu R Y, Sun X Y, et al. Multi-static ISAC based on network-assisted full-duplex cell-free networks: performance analysis and duplex mode optimization. Sci China Inf Sci, 2025, 68: 150303
9 Pan Y, Li R, Da X, et al. Cooperative trajectory planning and resource allocation for UAV-enabled integrated sensing and communication systems. IEEE Trans Veh Technol, 2024, 73: 6502–6516
10 Jing X, Liu F, Masouros C, et al. ISAC from the sky: UAV trajectory design for joint communication and target localization. IEEE Trans Wireless Commun, 2024, 23: 12857–12872
11 Lyu Z, Zhu G, Xu J. Joint maneuver and beamforming design for UAV-enabled integrated sensing and communication. IEEE Trans Wireless Commun, 2023, 22: 2424–2440
12 Khalili A, Rezaei A, Xu D, et al. Efficient UAV hovering, resource allocation, and trajectory design for ISAC with limited backhaul capacity. IEEE Trans Wireless Commun, 2024, 23: 17635–17650
13 Wang Y, Zu K, Xiang L, et al. ISAC enabled cooperative detection for cellular-connected UAV network. IEEE Trans Wireless Commun, 2025, 24: 1541–1554
14 Chai R, Cui X, Sun R, et al. Precoding and trajectory design for UAV-assisted integrated communication and sensing systems. IEEE Trans Veh Technol, 2024, 73: 13151–13163
15 Meng K, Wu Q, Ma S, et al. UAV trajectory and beamforming optimization for integrated periodic sensing and communication. IEEE Wireless Commun Lett, 2022, 11: 1211–1215
16 Liu S, Liu R, Lu Z, et al. Cooperative cell-free ISAC networks: joint BS mode selection and beamforming design. In: Proceedings of IEEE Wireless Communications and Networking Conference (WCNC), 2024. 1–6
17 Zhang R, Zhang Y, Tang R, et al. A joint UAV trajectory, user association, and beamforming design strategy for multi-UAV-assisted ISAC systems. IEEE Internet Things J, 2024, 11: 29360–29374
18 Gao Q, Zhong R, Liu Y. Trajectory and beamforming optimization in UAV-enabled ISAC system. In: Proceedings of IEEE Global Communications Conference (GLOBECOM), 2024. 1527–1532
19 Pang X, Guo S, Tang J, et al. Dynamic ISAC beamforming design for UAV-enabled vehicular networks. IEEE Trans Wireless Commun, 2024, 23: 16852–16864
20 Pei F, Xiang L, Klein A. Joint optimization of beamforming and 3D array-steering for UAV-aided ISAC. In: Proceedings of IEEE International Conference on Communications (ICC), 2024. 1249–1254
21 Zhou S, Yang H, Xiang L, et al. Temporal-assisted beamforming and trajectory prediction in sensing-enabled UAV communications. IEEE Trans Commun, 2025, 73: 5408–5419
22 He Z, Xu W, Shen H, et al. Full-duplex communication for ISAC: joint beamforming and power optimization. IEEE J Sel Areas Commun, 2023, 41: 2920–2936
23 Xu Y M, Xu D F, Xie Z Y, et al. Resolution-aware beam scanning for joint detection and communication in ISAC systems. Sci China Inf Sci, 2025, 68: 150305
24 Shang F, Du H H, Yang P L, et al. Measuring discrete sensing capability for ISAC via task mutual information. Sci China Inf Sci, 2025, 68: 150308
25 Wu Q, Zeng Y, Zhang R. Joint trajectory and communication design for multi-UAV enabled wireless networks. IEEE Trans Wireless Commun, 2018, 17: 2109–2121
26 Yuan X, Jiang H, Hu Y, et al. Joint analog beamforming and trajectory planning for energy-efficient UAV-enabled nonlinear wireless power transfer. IEEE J Sel Areas Commun, 2022, 40: 2914–2929
27 Lin H, Zhang Z, Wei L, et al. A deep reinforcement learning based UAV trajectory planning method for integrated sensing and communications networks. In: Proceedings of IEEE Conference on Vehicular Technology (VTC), 2023. 1–6
28 Zhang J F, Lu W D, Xing C W, et al. Intelligent integrated sensing and communication: a survey. Sci China Inf Sci, 2025, 68: 131301
29 Duan X Y, Zhang X Q, Xia S Q, et al. Machine learning empowered UAV-based beamforming design in ISAC systems. Sci China Inf Sci, 2025, 68: 150307
30 Pan C, Ren H, Wang K, et al. Multicell MIMO communications relying on intelligent reflecting surfaces. IEEE Trans Wireless Commun, 2020, 19: 5218–5233
31 Moon S, Liu H, Hwang I. Joint beamforming for RIS-assisted integrated sensing and secure communication in UAV networks. J Commun Netw, 2024, 26: 502–508
32 Pang X, Zhao N, Tang J, et al. IRS-assisted secure UAV transmission via joint trajectory and beamforming design. IEEE Trans Commun, 2022, 70: 1140–1152
33 Deng D, Zhou W, Li X, et al. Joint beamforming and UAV trajectory optimization for covert communications in ISAC networks. IEEE Trans Wireless Commun, 2025, 24: 1016–1030
34 Sankar R S P, Chepuri S P, Eldar Y C. Beamforming in integrated sensing and communication systems with reconfigurable intelligent surfaces. IEEE Trans Wireless Commun, 2024, 23: 4017–4031
35 Li S, Du H, Zhang D, et al. Joint UAV trajectory and beamforming designs for RIS-assisted MIMO system. IEEE Trans Veh Technol, 2024, 73: 5378–5392
36 Ge L, Dong P, Zhang H, et al. Joint beamforming and trajectory optimization for intelligent reflecting surfaces-assisted UAV communications. IEEE Access, 2020, 8: 78702–78712
37 Xiu Y, Lyu W, Yeoh P L, et al. Improving physical-layer security in ISAC-AAV system: beamforming and trajectory optimization. IEEE Trans Veh Technol, 2025, 74: 3503–3508
38 Zhang X, Peng M, Liu C. Sensing-assisted beamforming and trajectory design for UAV-enabled networks. IEEE Trans Veh Technol, 2024, 73: 3804–3819
39 Song X X, Fang Y, Wang F, et al. An overview on IRS-enabled sensing and communications for 6G: architectures, fundamental limits, and joint beamforming designs. Sci China Inf Sci, 2025, 68: 150301
40 Zhao C S, Zhang J H, Zhang Y X, et al. BUPTCMCC-6G-CMG+: a GBSM-based ISAC standard channel model generator. Sci China Inf Sci, 2025, 68: 150304
41 Liu X, Liu Y, Liu Z, et al. Fair integrated sensing and communication for multi-UAV-enabled Internet of Things: joint 3-D trajectory and resource optimization. IEEE Internet Things J, 2024, 11: 29546–29556